Angewandte Chemie
Eine Zeitschrift der Gesellschaft Deutscher Chemiker

Supporting Information

69451 Weinheim, Germany

Supplementary Information for

Nanoscale Corona Discharge in Liquids Enabling Nanosecond Optical Emission Spectroscopy

David Staack, [1] Alexander Fridman,[1] Alexander Gutsol[2], Yury Gogotsi,[3]* Gary Friedman[4]

[1]Department of Mechanical Engineering and Mechanics, Drexel University, Philadelphia, PA 19104, USA
[2] Chevron Energy Technology Corporation, 100 Chevron Way, 45-2143, Richmond, CA 94802. Previously at Department of Mechanical Engineering and Mechanics Drexel Univerisity,
[3]Department of Materials Science and Engineering Drexel University, Philadelphia, PA 19104, USA,
[4]Department of Electrical and Computer Engineering, Drexel University, Philadelphia, PA 19104, USA
*To whom correspondence should be addressed. E-mail: Gogotsi@drexel.edu

Materials and Experimental

Discharge Generation

A schematic of the electrical circuit used to generate the discharge pulses is shown in Figure S1. A pulsed power supply was constructed using spark gaps in a configuration similar to those used in other pulse generator systems (*1*). A direct current (DC) power supply (Bertran Model 205A -50R) capable of 50 kV output and reversible polarity was connected to a *RC* charging circuit. The DC circuit charges the capacitor until the voltage is sufficient to cause breakdown across the primary spark gap, SG1. The length of SG1 determines the voltage applied to the load. A current transformer (Pearsons model 2877) and voltage probe divider (North Star PVM-4) were used to estimate the current and voltage to the electrode. The voltages and currents measured by the probes may not precisely be that experienced by the electrode due to complications regarding the high frequency components of the pulses, bandwidth of the probes, parasitic losses, and displacement currents. The *R*, *C*, and power supply voltage, V_{ps}, determine the repetition rate of the discharge which was typically between 1 and 50 Hz. A second adjustable spark gap, SG2, acts to remove the voltage from the load. Variation of the length of SG2 adjusts the duration of the pulse. If SG2 is longer than SG1, the 2nd spark gap does not fire and the circuit operates in a stepped voltage rather than pulsed voltage mode. The operation of the pulsing circuit is largely independent of the load as only a small fraction of the power goes to the load. In stepped mode all of the power must dissipate through the liquid and the waveforms are highly dependent on the conductivity of the solution and immersed electrode geometry.

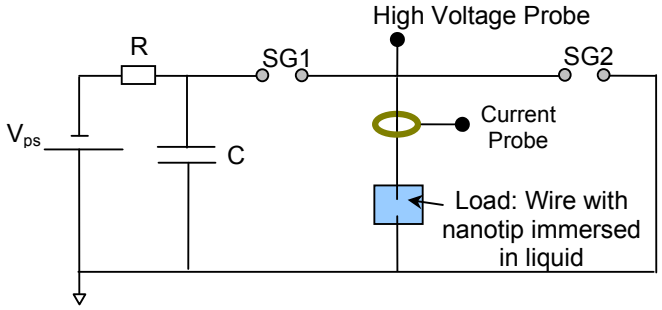

Figure S1. Schematic of the electrical circuit used for generating tens ns duration kV voltage pulses.

Figure S2 shows plots of the voltage, *V*, and current, *I*, measurements for various stepped and pulsed discharges and comparisons of the energy and power evolution in the discharges. Figure S2A shows the measurements for a 5 kV negative voltage step in a 0.1 mM NaCl solution with a 100 nm tip and approximately 1cm of lead wire immersed in the liquid. The voltage rapidly rises to 5 kV in about 10 ns corresponding to a 500 V/ns rise. All the power flows through the load in about 2 μs. Current behaves similarly with a peak in this case of about 20 A. Figure S2B shown the measurements for a 5 kV negative voltage pulse of 10 ns in duration (determined by the full width at half maximum (FWHM) of the voltage pulse). The initial voltage and current rise is nearly identical to that of the stepped voltage however the second spark gap is seen to abruptly remove the voltage and power from the tip. The rate of voltage removal is about 450 V/ns similar to the voltage application. Some ringing is noted in the non-optimized electric circuit after the termination of the voltage pulse. Waveforms for 26 ns and 60 ns pulse widths are shown in Fig. 2C and Fig. 2D. Power and energy were calculated for all cases. For the stepped voltage cases corresponds to 87% of the energy stored on the capacitor. The 10 ns pulse has an energy of 0.84 mJ/pulse. The energy and power evolution (Figures S2E and S2F) of the pulsed discharges is seen to follow that for stepped discharges up until the point of the 2nd spark gap firing. Similar features were seen for the light emission temporal profiles (Fig. 3B). The measurements shown in figure S2 are indicative of the pulsing control of the power supply and do not correspond to the minimum sized discharges. For the smallest NCDP voltages were 3kV and max currents were 1A corrsponding to only very small field emission overvoltages and powers of about 0.1 mJ/pulse. Such low voltages could only be attained on new probe

tips though they could be operated repeatedy if low power was maintained. A single higher power pulse (>10mJ/pulse) would increase the radius of the probe tip and prevent operation at the lowest voltages.

A photo of the experimental setup is shown in figure S3 and illustrates the compact size of the system especially in comparison to portable LIBS systems (*2*). The size of an optimized discharge generator could be several cm and system size would likely be limited by the light detection apparatus (a portable fiber optic spectrometer).

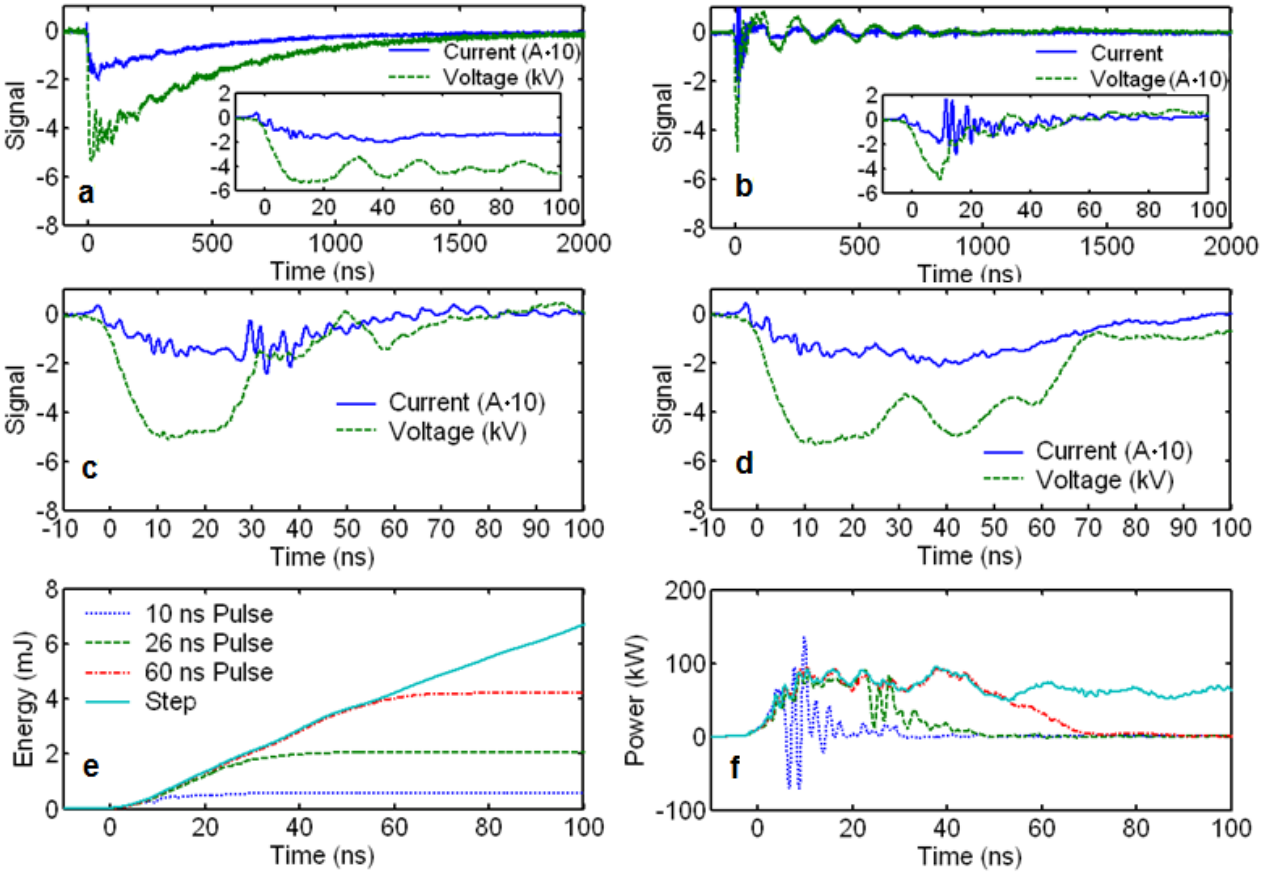

Figure S2: Measured voltage and current for (a) stepped voltages and pulsed voltages of (b) 10 ns, (c) 26 ns and (d) 60 ns durations. Comparison of the (e) energy and (f) power during the discharge pulse.

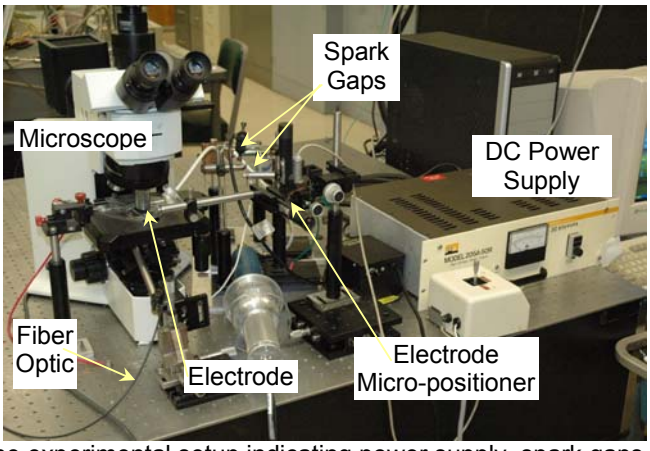

Figure S3: Photograph of the experimental setup indicating power supply, spark gaps, electrode, and microscope (spectrometer not shown).

Nano-scale Probes

Several varieties of micro-scale and nano-scale electrodes were used as probes. Fig. S4A shows an SEM image of the commercially available (T-4-10**,** GGB Industries, Inc.**)** electrolytically etched tungsten probe with <100 nm tip radii. Figure S4B shows an optical micrograph of several of the carbon fibers with approximately 4 μm diameter manufactured by Energy Science Laboratories, Inc. The inset Figure S4C shows a single fiber. Figure S5A shows a carbon nanotubes attached to the

substrate (template grown noncatalytic CVD CNTs of ~200 nm diameter (*3*)) these nanotubes were used as remote electrodes both dispersed in liquid (Fig 1) and electrostatically affixed to a polyacrylonitrile (PAN) coating (*4*) as shown in this figure. Figure S5B shows a carbon nanotube placed inside and affixed to the end of a pulled glass capillary (*5*) useful for manipulation and probing using a single nanotube.

Collection and Analysis of Optical Emission Spectra

All spectra were acquired using one stage of a TriVista scanning monochromator system from Princeton Instruments. Light from the discharge was collected by a single optical fiber of 3 m in length and 250 μm in diameter aligned with the discharge and mounted on the entrance slit of the spectrometer. Optical emission spectra (OES) of the discharge were taken in a range 200–900 nm averaging emission from the entire discharge. Either an 1800 g/mm, 1100 g/mm or 900 g/mm grating was used depending on the spectral range and resolution required. An intensified CCD camera (Princeton Instruments Gen III PI-MAX 2) was mounted on the exit of the spectrometer to digitally record the spectra. A photon counting photomultiplier tube (R928, Hamamatsu**)** was mounted on the secondary spectrometer output in order to verify results from and to calibrate the ICCD camera intensity.

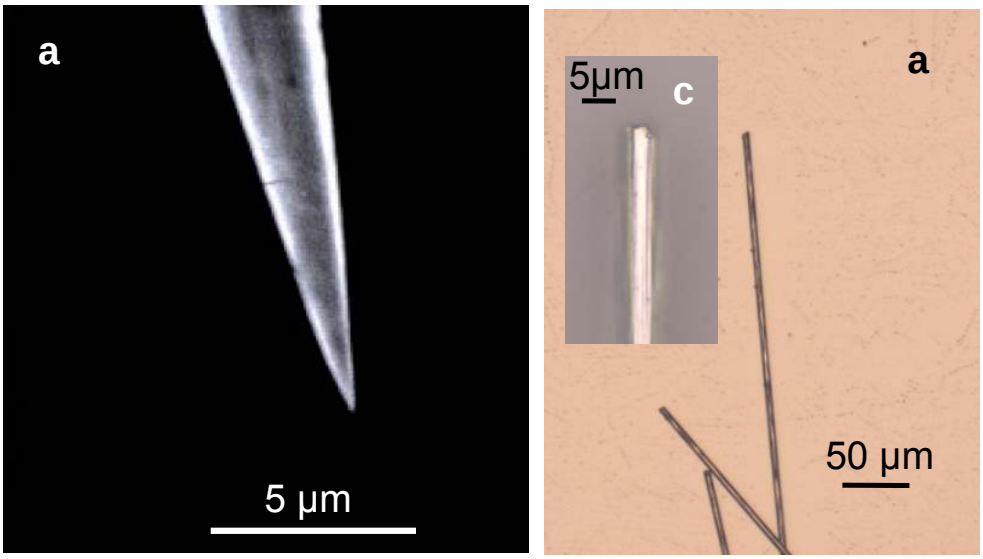

Figure S4: Images of electrode probes. a) SEM image of 100 nm tip of tungsten probe used as electrode. b) and c) ~ 4 μm diameter carbon fibers.

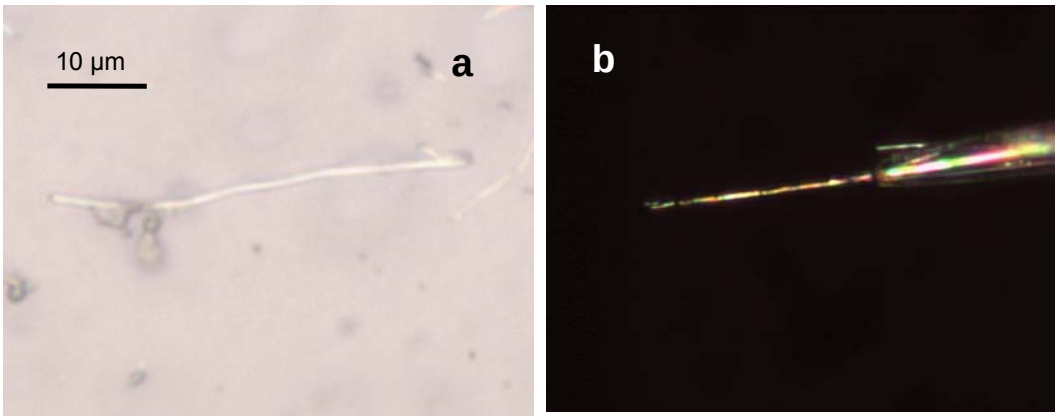

Figure S5: Images of carbon nanotubes used as probes. a) Template grown nanotubes affixed to a polymer film. b) The same kind of carbon nanotube (~200 nm in diameter) placed inside a glass pipette with a ~1 μm tip (courtesy J. Freedman).

Temporally resolved spectra shown in Figure S6 were acquired using externally triggered programmable gating of the ICCD camera. The camera was typically triggered by the electro-magnetic interference (EMI) generated by the first spark gap picked up using an ~2 cm antenna (this trigger signal was used as it has no associated cabling delay as in the case for the measured voltage signal). The gating width was programmable between 25 ns and several μs and the pulse timing generator (PTG) has a minimum insertion delay of 25 ns. Additional delays both in the signal and gating were accounted for when

considering the timing budget of the light collection. Typically as shown in Figures S6 and figure 3A this results in the light collection beginning after the initiation of light emission. A second timing configuration tested uses a modification of the circuit to add an additional spark gap in series before the first spark gap which effectively acts as a pre-trigger for the voltage pulse on the probe. A comparison of time resolved spectra using the EMI trigger and the pre-trigger is shown in Figure S7. This indicates that while some information regarding the rise of the initial emission phase is lost it is not significant. The pre-trigger configuration however was somewhat more cumbersome to adjust the pulse height and duration and was not used in most experiments.

Multiple accumulations were used to acquire clean spectra. Both hardware (on CCD) and software accumulations were used. The number of accumulations used depended on the intensity of light emission. For the smallest discharge and low concentration species several hundred to thousands of accumulations were typically used. Total acquisition times over a single spectral range for 1000 pulses though were typically less than one minute. In order to more accurately determine the peak height and width, Lorentzian line shapes were fit to the experimentally measured spectra. Peak location is used to identify what species a particular observed transition belongs to by comparison with databases (*6*). Peak height are proportional to species concentration but are also highly dependant on the electron excitation temperature, emission constants for that transition, and the degree to which excited states are quenched by non-radiative or collisional mechanism. Common Boltzmann plots of relevant line intensities were used to estimate the electronic excitation temperature at about 0.5 eV.

The narrow line widths observed in our nanoscale discharges are essential to their usefulness as probes for elemental analysis. The line widths also give information about the conditions of the plasma discharge. Considering that little is known about the state and phase of the plasma region relevant mechanism that might contribute to the line widths are instrumental broadening, thermal Doppler broadening, and collisional broadening including Van der Waals, and Stark broadening (*7*). Determined line widths are shown in Figure S8 corresponding to spectra in Figure S6 and the peak heights in Figure 3A.

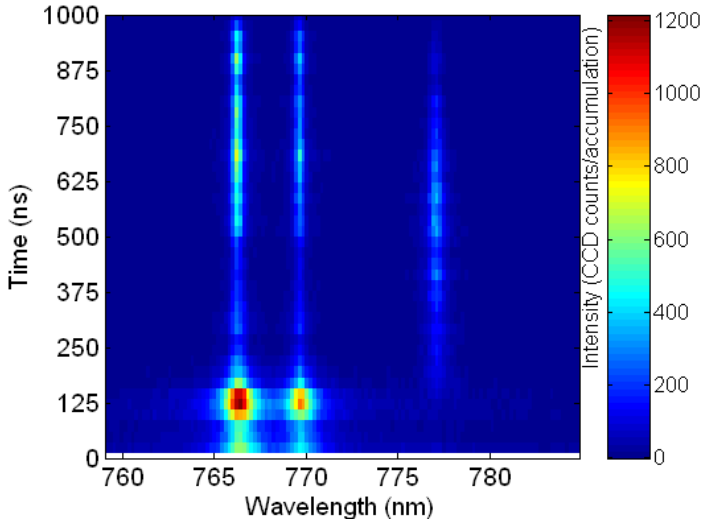

Figure S6: Time resolved spectra with 25 ns resolution of 10mM KCl aqueous solution. Spectral range shows simultaneous acquisition of three peaks: two due to K (766.5, 769.9) and a single peak due to O (triplet around 777.4).

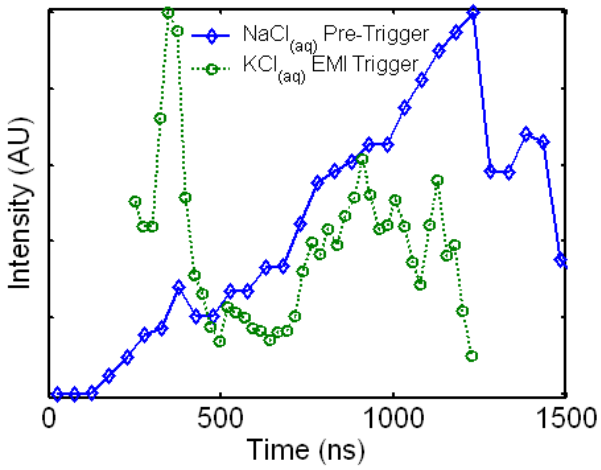

Figure S7: Time resolved peak heights comparing use of a pre-trigger and spark gap EMI as triggers for the spectral data collection.

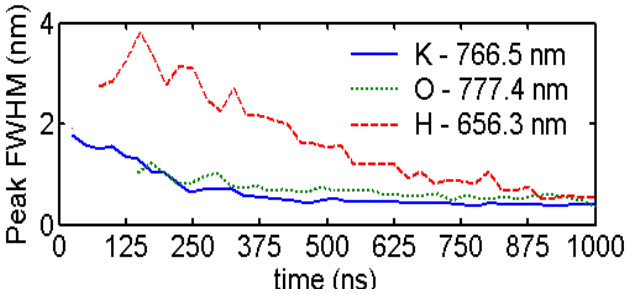

Figure S8: Temporal evolution of determined line width which is indicative of electron density for 9kV stepped voltages in 10 mM KCl aqueous solution. Potassium and oxygen data correspond to profiles shown in Figure S4.

In this experiment, an instrumental broadening of about 0.35 nm was measured. The remainder of the broadening between <0.1 and 3.5 nm is due to the conditions of the plasma. Considering the hydrogen Balmer α line, the smallest broadening ~0.1 nm if due to solely one of these effects would required a temperature of 45000 K, a number density in the range of 0.87 $x10^{27}$ to $2.7x10^{27}$ cm^{-3} (assuming temperatures in range of 300 K to 10000 K), or an electron density of $2x10^{15}$ cm^{-3} for Doppler, Van der Waals, and Stark broadening respectively. Such temperatures are not realistic also the Lorentzian line shape is consistent with collisional broadening. The bulk number density, which is in the range of 2% to 8% of the number density of liquid water or greater than 30 atmospheres if considering an ideal gas, is also probably not the broadening source. The electron density estimate, Figure S9, is physically most likely and if the broadening is attributed to electron density variations the maximum broadening corresponds to an electron density of about $7x10^{17}$ cm^{-3}. The minimum broadening measured for this discharge corresponds to electron densities less than 10^{16} in the relaxation phase of the discharge. Conditions in this case were for a 9 kV voltage step in a 10 mM KCl aqueous solution. This concentration was carefully chosen by several trials so that K and O peaks would be of similar height during the evolution of the discharge. Since stepped voltages were used the probe tip was likely slightly larger than the initial 100 nm. The reason for the observed discrepancy in trends between the H and K line width in unclear it may be due to different regions of light emission and spatial variations in electron density, also the K and H peaks could not be measured simultaneously and especially for stepped voltage pulses there may be some slight degradation of the probe tip shape resulting in different temporal evolution of the discharge. Lower electron densities were measured in lower voltage nanosecond duration pulses with lowest electron densities corresponding to widths less than the instrumental broadening ~10^{15} cm^{-3}.

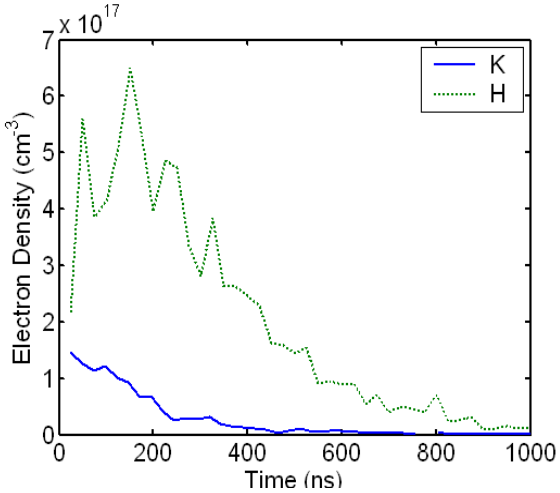

Figure S9: Time resolved electron density estimated from line width due to Stark broadening using the hydrogen Balmer alpha and Potassium lines shown in Figure S6.

Additional Data

Optical emission spectra for various elements and conditions

In addition to the spectra containing sodium, potassium, calcium, and magnesium, which were shown in the article, spectra corresponding to several other elements were also observed as shown in Figures S8 and S9 for lead, zinc, and gallium. Similar to LIBS, all elements with typical emission spectra in the optical range should be detectable. Spectra could be attained using either nano-scale nano-second duration discharges or micro-scale micro-second duration discharges. In general, nano-scale spectra were less intense and detection limits were often photon and signal-to-noise level limited. On the other hand, for micro-scale discharges detection limits could also be affected by interference from broadened hydrogen Balmer lines and

overlap with the OH (A-X) system. For the Pb spectra, detection limits were about 9 ppm using 100 pulses which is comparable to state of the art LIBS techniques (*8*) and may be improved by simply increasing the accumulation time. Stronger discharges of 15 kV, (~ 200 mJ/pulses) were used to collect the gallium spectra and tungsten emission lines were visible, likely due to degradation of the wire probe tip. For less intense pulses, no tungsten peaks were visible. For higher power discharges, 20 J/pulse, and macro-scale electrodes (similar to traditional macro-scale streamer-corona discharges in water) the spectra are dominated by broadened hydrogen spectral lines as shown in Figure S10 and preclude elemental analysis. This stresses once again the importance of using nanoscale probes.

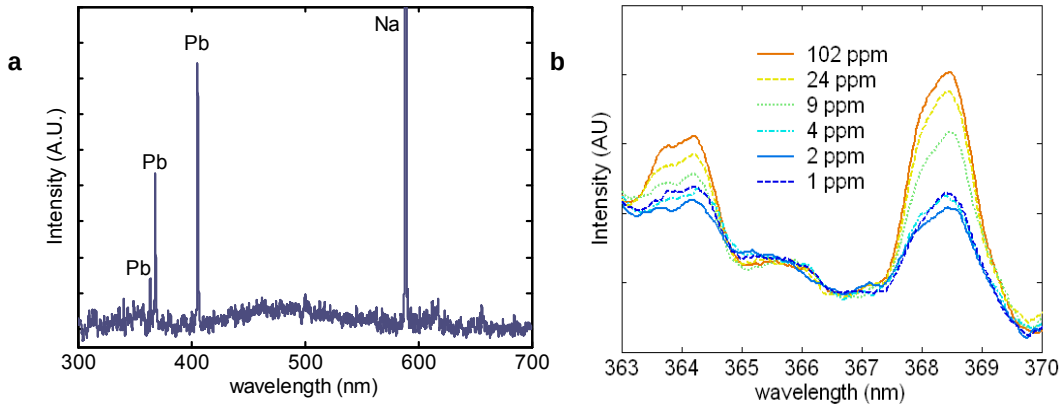

Figure S8: Optical emission spectra for lead containing solutions. a) Broad range scan indicating three common Pb peaks at 363.9 nm, 368.3 nm and 405.8 nm and sodium. b) Initial test indicate detection limits for micro-scale coronas to be about 9 ppm. Intensity response in non-linear due to solubility limits of lead in sodium chloride containing solutions.

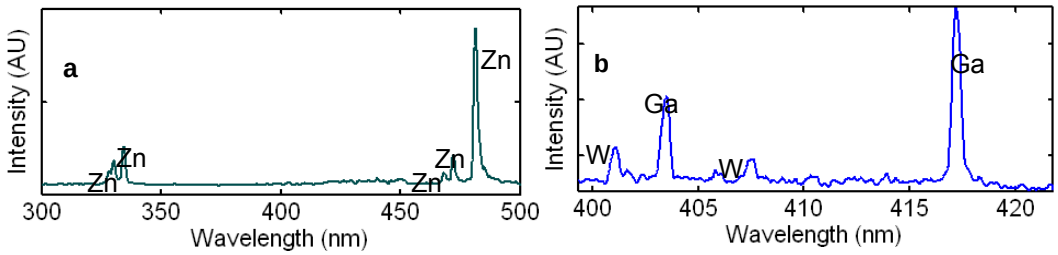

Figure S9: Optical emission spectra for a zinc sulfate solution (a), indicating Zn peaks at 328.2 nm, 330.3nm, 334.5 nm, 468.8 nm, 472.2 nm, 481.1 nm, and (b) a gallium containing solution with 0.2 J/pulse discharges, indicating gallium peaks and tungsten peaks due to probe tip degradation.

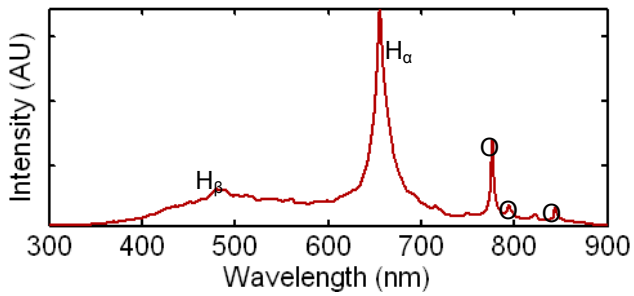

Figure S10: Spectrum for high power 20 J/pulse streamer corona in water indicating significant line broadening corresponding to electron densities greater than 10^{18} cm^{-3}.

References

1. J. Mankowski, *IEEE Transactions on Plasma Science* **28**, 102 (2000).
2. M. Ferretti *et al.*, *Spectrochimica Acta Part B* **62**, 1512 (2007).
3. D. Mattia, H. H. Bau, Y. Gogotsi, *Langmuir* **22**, 1789 (2006).
4. M. Havel, K. Behler, G. Korneva, Y. Gogotsi, *Advanced Functional Materials*, in press (2008).
5. J. R. Freedman *et al.*, *Applied Physics Letters* **90**, 103108 (2007).
6. Y. Ralchenko, A. E. Kramida, J. Reader. (National Institute of Standards and Technology, Gaithersburg, MD, 2008).
7. H. R. Griem, *Spectral Line broadening by plasmas* (Academic Press, New York, 1974).
8. Y. Godwal, S. L. Lui, M. T. Taschuk, Y. Y. Tsui, R. Fedosejevs, Spectrochimica Acta Part B 62, 1443 (2007).